Controlling limit-cycle behaviors of brain activity

J. W. Kim[1,2] and P. A. Robinson[1,2,3]
[1]*School of Physics, The University of Sydney, Sydney, New South Wales 2006, Australia*
[2]*Brain Dynamics Center, Westmead Millennium Institute, Westmead Hospital and Western Clinical School of The University of Sydney, Westmead, New South Wales 2145, Australia*
[3]*Faculty of Medicine, The University of Sydney, Sydney, New South Wales 2006, Australia*
(Received 8 April 2007; revised manuscript received 24 October 2007; published 19 May 2008)

The limit cycles of brain activity are studied using a compact continuum model that reproduces the main features of electroencephalographic signals, including bifurcations of fixed points and limit cycles in seizures. Frequencies and amplitudes are predicted analytically and related to physiology. Gaussian stimuli yield two distinct evoked responses in the linearly stable zone, consistent with experiment. Limit cycles can be initiated or suppressed by control signals or stimuli.

DOI: 10.1103/PhysRevE.77.051914 PACS number(s): 87.19.L−, 87.19.R−, 05.45.−a

I. INTRODUCTION

Much effort has been devoted to understanding complex brain dynamics, often observed using electroencephalograms (EEGs) resulting from cortical electrical activity [1–3]. EEGs in epilepsy, Parkinson disease, and related conditions show limit-cycle dynamics due to coherent collective behavior (synchrony) of neurons [4,5], while healthy EEGs are mostly unsynchronized [6]. It has thus been suggested that control of synchrony of populations of neurons could provide a therapy for neural disorders associated with abnormal synchrony [7–10], which include essential tremor, sleep-related movement disorders, flickering hallucinations in migraine, and Charles Bonnet syndrome [11–13]. Control might be attained via stimuli applied via a control loop, as an alternative treatment for the above disorders. These long-term aims require synchronous behavior to be related explicitly to its physiological basis.

To study epileptic limit cycles and increase insight into factors underlying their potential control, we use a recent physiologically based compact mean-field model for dynamics of the coupled cortex and thalamus [14], which describes the relevant brain activity via a second-order delay differential equation for the cortical excitatory activity, following approaches developed since the 1970s ([15] and references therein). The model includes key physiological features such as corticocortical propagation and delayed feedbacks via subcortical pathways, discussed in detail previously [14]. When driven by noise, the model reproduced and unified many properties of EEGs (e.g., spectral peaks, epileptic dynamics) in a physiologically plausible parameter region with greater simplicity than previous studies [17,18]. It can be further linked to physiological experiments via its connection to previous models whose parameters have been calibrated against clinical outcomes [15]; a detailed comparison is given in [14].

Here we characterize epileptic limit cycles, frequencies, and amplitudes in terms of the strengths of corticocortical coupling and delayed subcortical feedback, which relates the dynamical origin of the limit cycles to physiologically measurable quantities. We further probe limit-cycle behaviors by applying short external stimuli. Linear model responses are consistent with experimental evoked responses (ERs) [19–22]. We demonstrate that epileptic cycles outside the linearly stable zone can be suppressed by applying discrete stimuli, as proposed in other contexts [7–10]. When a limit cycle and fixed point coexist, we show the cycle can be initiated by a stimulus, providing a mechanism for reflex (e.g., photosensitive) epilepsy [23]. Our physiologically based model thus provides a step forward studying neuronal synchrony and its mechanisms, potentially relevant to the above disorders.

II. COMPACT MODEL FOR BRAIN ACTIVITY

Model equation. Since temporal dynamics is of interest in this work, we model electrical activity at the scalp introducing the nondimensional quantities: spatially homogeneous field $\psi(\tau)$ (a perturbation to a state of the system) and $\tau=\gamma t$, where γ is a decay rate of the field [14,16]. The relevant model equation is [14]

$$d^2\psi(\tau)/d\tau^2 + 2d\psi(\tau)/d\tau = c_1\psi(\tau) + \epsilon_2\psi^2(\tau) + \epsilon_3\psi^3(\tau) + c_2\psi(\tau-\tau_0) + c_3\psi_n(\tau-\tau_0/2), \quad (1)$$

where $c_1\psi(\tau)$, $\epsilon_2\psi^2(\tau)$, and $\epsilon_3\psi^3(\tau)$ ($\epsilon_3<0$) represent linear and nonlinear activity due to cortical neurons, $c_2\psi(\tau-\tau_0)$ denotes delayed feedbacks via a subcortical loop, and τ_0 is the loop delay. The stimulus $c_3\psi_n(\tau-\tau_0/2)$ is delayed at the cortex by $\tau_0/2$ since it is applied to the thalamus. The stimulus can be further approximated by white noise $\eta(\tau)$ in many situations [$\langle\eta(\tau)\rangle=0$ and $\langle\eta(\tau)\eta(\tau')\rangle=\delta(\tau-\tau')$, where angular brackets denote an average over τ]. c_j and ϵ_j can be written directly in terms of neural gains or firing rates and densities and strengths of connections, while $\tau_0=\gamma t_0 = vt_0/r_e$, t_0 is the dimensional loop delay, and v and r_e are the mean cortical signal velocity and range of long-range corticocortical axons (see Ref. [14] for a detailed discussion of these parameter values and their connections to the underlying physiology).

Steady states and stabilities. For $\tau_0=0$, the system [Eq. (1)] has a fixed point $(\psi, d\psi/d\tau)=(0,0)$, which becomes unstable when $c_1+c_2>0$ (zero-frequency instability). For τ_0

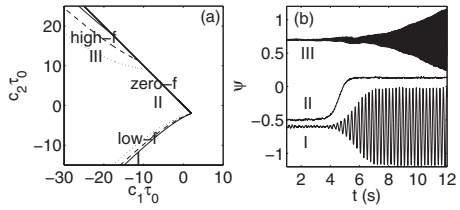

FIG. 1. (a) Stable zone [from (2) and (3)] and (b) numerical solutions of Eq. (1) while the system crosses the instability boundaries at $t=3$ s. The zero-frequency boundary (thick solid line) is independent of τ_0, while low- and high-frequency boundaries depend on τ_0: thin solid line ($\tau_0=8$), dashed line ($\tau_0=4$), and dotted line ($\tau_0=2$). In (b), $\tau_0=8$ and $\gamma=100$ s^{-1} [15].

>0, the fixed point bifurcates to a limit cycle when $c_1>c_p$ [14], with c_p and ω satisfying

$$c_p = -\omega^2 + 2\omega/\tan\omega\tau_0, \tag{2}$$

$$2\omega + c_2 \sin\omega\tau_0 = 0. \tag{3}$$

When $c_2<0$ a low-frequency ($\omega\tau_0\leq\pi$) instability occurs, whereas a high-frequency ($\pi<\omega\tau_0\leq 2\pi$) instability occurs for $c_2>0$ [Fig. 1(a)]. For our parameter values, zero-, low-, and high-frequency instabilities correspond to slow-wave, θ, and α instabilities in electrophysiological terminology. Figure 1(b) demonstrates the emergence of limit cycles when the system leaves the stable zone. Using an initial "perturbed" state [$\psi(\tau)=\psi^*+\eta$ for $-\tau_0\leq\tau<0$, where ψ^* is a fixed point of Eq. (1) and η is a small random number], we obtain limit cycles at 4.3 and 11.5 Hz [I and III in Fig. 1(b)], corresponding to θ (3–7 Hz) and α (8–12 Hz) rhythms.

Frequencies and amplitudes of limit cycles. In the limit-cycle regime, the solution of Eq. (1) is

$$\psi(t) \approx \psi_{\max}\cos\omega\tau + \psi_0, \tag{4}$$

where ψ_0 is the nonzero base line of the oscillation. Inserting Eq. (4) into Eq. (1), we obtain equations for the frequency ω, amplitude $\psi_{\max}$, and base line ψ_0 of the limit cycle from cosine and sine Fourier transforms of Eq. (1), giving

$$\psi_{\max}^2 = -\frac{4}{3\epsilon_3}\left(c_1 + \omega^2 - \frac{2\omega}{\tan\omega\tau_0} + 2\epsilon_2\psi_0 + 3\epsilon_3\psi_0^2\right), \tag{5}$$

where ω and ψ_0 are roots of Eqs. (3) and (6), respectively:

$$\left(c_1 + 2\omega^2 - \frac{4\omega}{\tan\omega\tau_0} + \frac{2\omega}{\sin\omega\tau_0} + \frac{4\epsilon_2^2}{3\epsilon_3}\right)\psi_0 + 5\epsilon_2\psi_0^2 + 5\epsilon_3\psi_0^3 - (2\epsilon_2/3\epsilon_3)(c_1 + \omega^2 - 2\omega/\tan\omega\tau_0) = 0. \tag{6}$$

When $c_1\to\infty$, we find $\psi_0\approx 2\epsilon_2/3|\epsilon_3|$ and $\psi_{\max}\approx\sqrt{4c_1/3|\epsilon_3|}$, from the dominant terms in Eqs. (5) and (6). Similarly, $\psi_0\approx 2\epsilon_2/3|\epsilon_3|$ and $\psi_{\max}\approx\sqrt{4c_2/3|\epsilon_3|}$ when $c_2\to\mp\infty$ (i.e., $\omega\tau_0\to\pi$ or 2π for low- or high-frequency regions, respectively). Figures 2(b) and 2(d) show $\psi_{\max}\sim\sqrt{c_1}(\sqrt{c_2})$, while $\psi_0\sim$const, which supports the above approximations. Dimensionless frequencies depend only on c_2, as seen from Eq. (3) and Fig. 2(c).

Bifurcations and hysteresis. Figure 3 shows attractors of Eq. (1) obtained as follows. For $\tau_0=0$, setting all derivatives

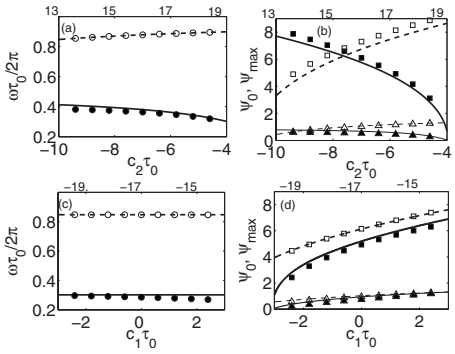

FIG. 2. Frequencies ω (○), amplitudes $\psi_{\max}$ (□), and base lines ψ_0 (△) of limit cycles from numerical solutions of Eq. (1) are compared with theoretical estimates from Eqs. (3), (5), and (6). Dotted and solid lines denote values in high- and low-frequency regions (P_h and P_l), respectively. (a) and (b) $c_1\tau_0=-20$, $13\leq c_2\tau_0\leq 19$ for P_h, and $c_1\tau_0=-3$, $-10\leq c_2\tau_0\leq -4$ for P_l. (c) and (d) $c_2\tau_0=13$, $-20\leq c_1\tau_0\leq -14$ for P_h, and $c_2\tau_0=-4$, $-3\leq c_1\tau_0\leq 3$ for P_l. $\tau_0=8$.

in Eq. (1) to zero, we find a trivial fixed point $\psi^*=0$ that is stable for $c_1<c_b=-c_2+\epsilon_2^2/4\epsilon_3$. For $\tau_0\neq 0$, seeking solutions of Eq. (1) of the form $\psi^* e^{\lambda\tau}$, we can obtain the critical point c_p where a limit cycle emerges [14]. Since this bifurcation is of most interest here, we restrict our analysis and numerics to the vicinity of c_p. Note that the system has nonzero fixed points, one stable and one unstable, for $c_1\geq c_b$. These fixed points can potentially be important for understanding certain electrophysiological activities of the brain, such as base-line shifts of EEG signals. However, in order to stress and focus on the main bifurcation feature (i.e., the emergence of limit cycles from a fixed point, mentioned above), we do not discuss the dynamical properties of other fixed points.

The amplitudes of the limit-cycle attractors [Eq. (5)] are shown as dashed lines in Figs. 3(a) and 3(b) for supercritical and subcritical bifurcations, respectively. From Eq. (6), ψ_0 can have up to three solutions for given parameters of the model [Eq. (1)]. $\psi_{\max}$ [Eq. (5)] thus has multiple values as well, yielding specific types of bifurcations. In particular, for a subcritical bifurcation [Fig. 3(b)], the system can have mul-

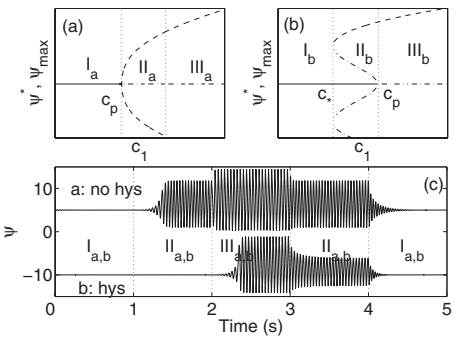

FIG. 3. Schematics of model bifurcations [(a) supercritical and (b) subcritical] and (c) hysteresis. In (a) and (b), solid lines denote stable fixed points obtained from Eq. (1) analytically, and dashed lines (dash-dotted lines) denote amplitudes of stable (unstable) limit cycles from Eq. (5). Dotted vertical lines are guides only. Text defines c_p and c_*. $\tau_0=8$.

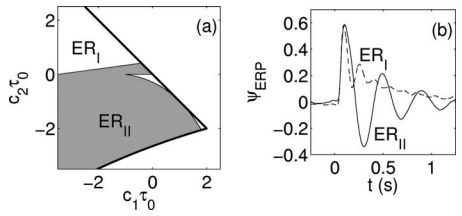

FIG. 4. (a) Phase diagram and (b) typical forms of ERs [obtained from Eq. (1)]. Thick solid lines in (a) are the instability boundaries from Fig. 1(a). The shaded area for ER_{II} is determined by the condition of Eq. (7) having a pole.

tiple attractors for $c_* \leq c_1 \leq c_p$, where c_* is a saddle node from which an additional unstable cycle emanates.

For a subcritical bifurcation [Fig. 3(b)], hysteresis is seen when the system loses and regains stability. For example, a system initially attracted to a fixed point [see I_b in Fig. 3(b)] can stay there although it moves into zone II_b where a fixed point and stable limit cycle coexist. However, the state bifurcates to a limit cycle as the system crosses the instability boundary to zone III_b. The limit cycle persists when the system moves into zone II_b again. The system regains its initial state once it returns to zone I_b, as seen in the bottom plot in Fig. 3(c). In contrast, the top plot in Fig. 3(c) shows no hysteresis because the bifurcation is supercritical.

Evoked responses. We now consider ERs to discrete Gaussian stimuli. In the stable zone, we linearize Eq. (1) and Fourier transform to get the transfer function [14]

$$\psi(\omega) = \frac{-e^{i\omega\tau_0/2}\psi_n(\omega)}{\omega^2 + 2i\omega + c_1 + c_2 e^{i\omega\tau_0}} \equiv \frac{-e^{i\omega\tau_0/2}\psi_n(\omega)}{\Omega^2(\omega)}, \quad (7)$$

where $\psi_n(\omega) = c_3 e^{-\sigma^2\omega^2/2}$ for $\psi_n(\tau) = c_3 e^{-\tau^2/2\sigma^2}$. Inverse transforming (7) yields

$$\psi_{ER} = \begin{cases} d_1 e^{-(\tau+\tau_0/2)^2/2\sigma^2}, \\ d_2 e^{-\omega_i(\tau+\tau_0/2)} \sin[\omega_r(\tau+\tau_0/2) + \delta], \end{cases} \quad (8)$$

where $d_{1,2}$ are constants, $\omega = \omega_r + i\omega_i$ (ω_r and ω_i are real), and $\delta = \delta(\omega_r, \omega_i)$ are determined by the condition $\Omega^2(\omega) = 0$, which gives explicit equations for ω_r and ω_i and yields Eqs. (2) and (3) when $\omega_i = 0$.

Figure 4 shows the phase diagram and typical ERs (gradually returning to the fixed point) obtained from our compact model (1). These forms—a damped resonance superposed on a long-lived shift (ER_I) and a damped resonance (ER_{II})—are consistent with previous literature [19–22], which shows good agreement with the approximation [Eq. (8)], apart from small nonlinear oscillations.

III. CONTROL OF LIMIT CYCLES

Equation (7) is invalid beyond the instability boundaries, where dynamics is locked to strong limit cycles. To investigate the effect of stimuli on these cycles, we apply two consecutive Gaussian stimuli $\psi_j = c_3 e^{-(\tau-T_j)^2/2\sigma^2}$ ($T_1 \approx 151\tau_0$, $T_2 \approx 305\tau_0$, $c_3 = 20$, and $\sigma \approx 0.1/\omega$) to each of two systems: (i) one has only one limit-cycle attractor [zone II_a, Fig. 3(a)], while (ii) the other has a limit-cycle attractor and fixed point

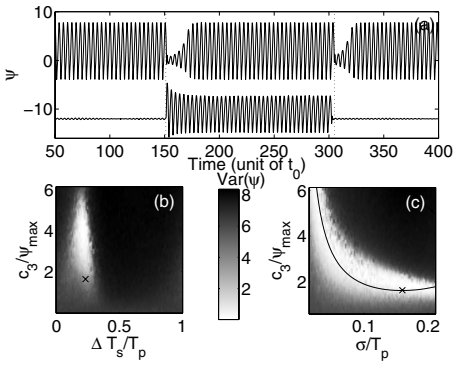

FIG. 5. Suppression and initiation of limit cycles by stimuli. Dotted lines denote the first and second stimuli. Suppression is quantified by the variance of ψ after stimuli, as shown in (b) and (c). Crosses and solid lines indicate optimal time ΔT_s, strength c_3, and width σ of the stimulus from (11) and (12); T_p and $\psi_{\max}$ are the period and amplitude of the cycle.

[zone II_b, Fig. 3(b)]. As shown in Fig. 5, limit cycles can be suppressed temporarily for (i) [top plot, Fig. 5(a)] because any perturbed state eventually returns to the limit cycle. However, suppression can be permanent for (ii) [bottom plot, Fig. 5(a)] because external stimuli can push the system to be attracted to a fixed point.

Similar techniques for suppressing Parkinsonian limit cycles have been proposed, based on generic phase oscillator descriptions of collective behavior. These showed that abnormal synchrony can be destroyed by a double-pulse stimulus [7] or delayed linear [8] or nonlinear [9] feedback. These authors suggested temporally structured and impulsive stimuli as a potential therapy for neural disorders with abnormal synchrony. Our method, based on a mean-field description of the dynamics of neuronal populations, will further facilitate such applications by providing more detailed connections to underlying mechanisms via its physiologically based parametrization.

We also observe initiation of limit cycles by a stimulus when the system has a subcritical bifurcation. The system, initially attracted to a fixed point, evolves to a limit cycle if a stimulus is strong enough to perturb the stability of the fixed point and push the dynamics to the periodic attractor (i.e., $c_3 \gg \psi_{\max}$). A similar stimulus-locked response occurs for two phase oscillators coupled by delayed feedback [10], but our result differs because we model neural fields, not just their phase.

This sudden emergence of stable limit-cycle behavior from a fixed point may explain reflex (e.g., photosensitive) epilepsies [23]. The system can regain its initial state when the second stimulus perturbs the limit-cycle attractor as shown in the lower plot in Fig. 5(a). One could also seek therapies or preventive measures (e.g., pharmacological) that widen the basin of attraction of the original fixed point or change the topology of the system to avoid the subcritical bifurcation structure.

Suppression of limit cycles requires fine-tuning because its effectiveness depends on parameters of stimuli, as for Parkinsonian tremors [9]. To find the optimal stimulus we apply similar methods as used to find $\psi_{\max}$, giving

$$(\psi_s^2 - p)\psi_s \approx qc_3\sigma e^{-\omega^2\sigma^2/2} \cos\omega(T_s + \tau_0/2), \quad (9)$$

$$-(2\omega + c_2 \sin\omega\tau_0)\psi_s \approx qc_3\sigma e^{-\omega^2\sigma^2/2} \sin\omega(T_s + \tau_0/2), \quad (10)$$

where T_s is the stimulus time, $p=4(\omega^2+c_1+c_2\cos\omega\tau_0)/3|\epsilon_3|>0$, and $q=4\sqrt{2\pi}/3|\epsilon_3|>0$ (we set $\epsilon_2=0$ for simplicity). The stimulus suppresses a limit cycle effectively if ψ_s obtained from Eqs. (9) and (10) is small.

Since ω is roughly independent of the stimulus [Fig. 5(a)], the left-hand side of Eq. (10) becomes zero due to Eq. (3), so $\omega(T_s+\tau_0/2)=n\pi$ for integer n. To have $\psi_s>0$, Eq. (9) requires $\cos\omega[(T_s+\tau_0/2)]<0$, so $\omega(T_s+\tau_0/2)\to(2n+1)\pi$. Thus, optimal timing relative to a cycle peak is

$$\Delta T_s = (2\pi - \omega\tau_0)T_p/4\pi, \quad (11)$$

from which $\Delta T_s \approx 0.23T_p$ ($T_p=2\pi/\omega$) for the given parameters [Fig. 5(b)]. A similar condition was found previously [18] where numerics demonstrated that, to suppress seizures, control stimuli should be applied slightly before a seizure signal reaches maximal negative polarity. Since external control stimuli are relayed to cortex with a time delay $\tau_0/2$ in our model, they should be applied $\tau_0/2$ earlier, as verified by numerics (Fig. 5) and Eq. (11).

Equation (9) has a positive solution only when

$$c_3 \le re^{\omega^2\sigma^2/2}/\sigma, \quad (12)$$

where $r=2(p/3)^{3/2}/|q\cos\omega(T_s+\tau_0/2)|$, which defines the area below the curve in Fig. 5(c). The right-hand side of Eq. (12) has a minimum $r\omega\sqrt{e}$ ($\approx 1.6\ \psi_{\max}$) when $\sigma=1/\omega$ ($\approx 0.16\ T_p$), which defines optimal c_3 and σ (Fig. 5). Figure 5 shows that ΔT_s is well estimated by Eq. (11), while c_3 is underestimated by Eq. (12), but within a factor of 2.

IV. CONCLUSION

We have probed limit-cycle behaviors of the brain and shown how they are modulated by physiological parameters and stimuli in linear and nonlinear regimes. As a prelude to more targeted modification, potentially via a control loop, we showed that limit cycles can be suppressed by stimuli and analyzed optimal stimulus times, strengths, and widths. Initiation of limit cycles by stimuli, resembling reflex epilepsy, was also discussed.

ACKNOWLEDGMENTS

We thank S. J. van Albada, H. Henke, and A. J. Phillips for their comments. The Australian Research Council supported this work.

[1] M. P. Stryker, Nature (London) **338**, 297 (1989).
[2] A. M. L. Coenen, Neurosci. Biobehav. Rev. **19**, 447 (1995).
[3] E. Niedermeyer and F. H. Lopes da Silva, *Electroencephalography: Basic Principles, Clinical Applications, and Related Fields*, 4th ed. (Williams and Wilkins, Baltimore, 1999).
[4] R. Llinas and H. Jahnsen, Nature (London) **297**, 406 (1982).
[5] D. Pare, R. Curro'Dossi, and M. Steriade, Neuroscience **35**, 217 (1990).
[6] A. Nini, A. Feingold, H. Slovin, and H. Bergmann, J. Neurophysiol. **74**, 1800 (1995).
[7] P. A. Tass, *Phase Resetting in Medicine and Biology: Stochastic Modelling and Data Analysis* (Springer, Berlin, 1999); P. A. Tass, Biol. Cybern. **85**, 343 (2001).
[8] M. G. Rosenblum and A. S. Pikovsky, Phys. Rev. Lett. **92**, 114102 (2004); Phys. Rev. E **70**, 041904 (2004).
[9] O. V. Popovych, C. Hauptmann, and P. A. Tass, Biol. Cybern. **95**, 69 (2006).
[10] V. Krachkovskyi, O. V. Popovych, and P. A. Tass, Phys. Rev. E **73**, 066220 (2006).
[11] G. Deuschl, J. Raethjen, R. Baron, M. Lindemann, H. Wilms, and P. Krack, J. Neurol. **247**, Suppl. 5, V/33 (2000); G. Deuschl and H. Bergman, Mov. Disord. **17**, Suppl. 3, S41 (2002).
[12] G. C. Brown and R. P. Murphy, Arch. Ophthalmol. **110**, 1251 (1992).
[13] R. Manni and M. Terzaghi, Neurol. Sci. **26**, s181 (2005); G. Mayer, J. Wilde-Frenz, and B. Kurella, J. Sleep Res. **16**, 110 (2007).
[14] J. W. Kim and P. A. Robinson, Phys. Rev. E **75**, 031907 (2007).
[15] P. A. Robinson, C. J. Rennie, D. L. Rowe, and S. C. O'Connor, Hum. Brain Mapp. **23**, 53 (2004); P. A. Robinson, C. J. Rennie, D. L. Rowe, S. C. O'Connor, and E. Gordon, Philos. Trans. R. Soc. London, Ser. B **360**, 1043 (2005).
[16] P. A. Robinson, C. J. Rennie, and J. J. Wright, Phys. Rev. E **56**, 826 (1997).
[17] P. A. Robinson, C. J. Rennie, and D. L. Rowe, Phys. Rev. E **65**, 041924 (2002); P. A. Robinson, C. J. Rennie, D. L. Rowe, S. C. O'Connor, J. J. Wright, E. Gordon, and R. W. Whitehouse, Neuropsychopharmacology **28**, S74 (2003).
[18] P. Suffczynski, S. Kalitzin, and F. H. Lopes da Silva, Neuroscience **126**, 467 (2004); P. Suffczynski, F. H. Lopes da Silva, J. Parra, D. Velis, and S. Kalitzin, J. Clin. Neurophysiol. **22**, 288 (2005).
[19] C. J. Rennie, P. A. Robinson, and J. J. Wright, Biol. Cybern. **86**, 457 (2002).
[20] H. Shibasaki, M. Nakamura, and S. Nishida, Electroencephalogr. Clin. Neurophysiol. **66**, 200 (1987).
[21] V. J. Samar, K. P. Swartz, and M. R. Raghuveer, Brain Cogn. **27**, 398 (1995).
[22] S. Makeig *et al.*, J. Neurosci. **19**, 2665 (1999).
[23] C. D. Binnie, in *Epilepsy: A Comprehensive Textbook*, edited by J. Engel and T. A. Pedley (Lippincott-Raven, Philadelphia, 1998), p. 2489; B. G. Zifkin and F. Andermann, in *Epilepsy: A Comprehensive Textbook*, edited by J. Engel and T. A. Pedley (Lippincott-Raven, Philadelphia, 1998), p. 2507.